

# Giant Enhancement of Photoluminescence Emission in WS<sub>2</sub>-Two-Dimensional Perovskite Heterostructures

Arky Yang,<sup>†,‡</sup> Jean-Christophe Blancon,<sup>‡,‡</sup> Wei Jiang,<sup>§</sup> Hao Zhang,<sup>‡</sup> Joelson Wong,<sup>†,‡</sup> Ellen Yan,<sup>†,‡</sup> Yi-Rung Lin,<sup>†</sup> Jared Crochet,<sup>‡</sup> Mercouri G. Kanatzidis,<sup>||</sup> Deep Jariwala,<sup>†,‡</sup> Tony Low,<sup>§</sup> Aditya D. Mohite,<sup>\*,‡</sup> and Harry A. Atwater<sup>\*,†</sup>

<sup>†</sup>California Institute of Technology, Pasadena, California 91125, United States

<sup>‡</sup>Department of Chemical and Biomolecular Engineering, Rice University, Houston, Texas 77005, United States

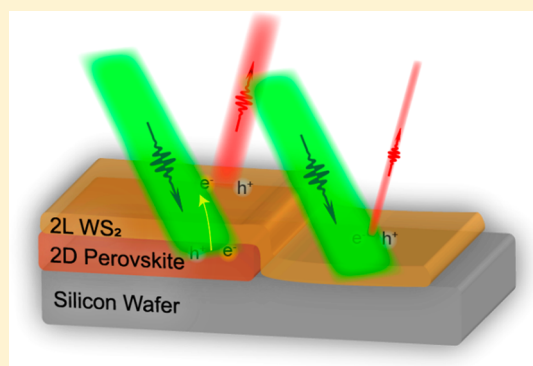
<sup>§</sup>Department of Electrical and Computer Engineering, University of Minnesota, Minneapolis, Minnesota 55455, United States

<sup>||</sup>Northwestern University, Evanston, Illinois 60208, United States

## S Supporting Information

**ABSTRACT:** Transition metal dichalcogenides (TMDCs) and two-dimensional organic and inorganic hybrid lead halide perovskites (2DPVSKs) have emerged as highly promising materials for ultralight and ultrathin optoelectronics application. They both exhibit tunability of electronic properties such as band structure, and they can form heterostructures with various types of two-dimensional materials for novel physical properties not observed in single components. However, TMDCs exhibit poor emission efficiency due to defect states and direct-to-indirect interband transition, and 2DPVSKs suffer from poor stability in ambient atmosphere. Here we report that fabrication of TMDC-on-2DPVSK heterostructures using a solvent-free process leads to novel optical transitions unique to the heterostructure which arise from the hybrid interface and exhibit a strong photoluminescence. Moreover, a two orders of magnitude enhancement of the photoluminescence as compared to bare WS<sub>2</sub> emission is observed. The TMDC on top of 2DPVSK also significantly improves the stability as compared to bare 2DPVSK. Enhanced emission can be explained by electronic structure modification of TMDC by novel interfacial interactions between TMDC and 2DPVSK materials, which shows promise of the heterostructure for high efficiency and stable optoelectronic devices.

**KEYWORDS:** Two dimensional materials, perovskite, transition metal dichalcogenide, heterostructure, interface, photoluminescence



As two-dimensional (2D) semiconductors, transition metal dichalcogenides (TMDCs) have emerged as highly intriguing materials in the fields of optics,<sup>1,2</sup> electronics,<sup>3,4</sup> catalysis,<sup>5</sup> and mechanics.<sup>6</sup> They also present some unique physical properties at the mono- and bilayer level, such as valley polarization effects that allows controlling of spin carriers by light polarization, and led to the development of the field of valleytronics in information processing. However, many optoelectronic applications of these materials are limited by their low photoluminescence quantum yield (PL QY), especially at multilayer thicknesses.<sup>7,8</sup>

Another family of 2D materials, organic–inorganic (hybrid) layered perovskite materials, have also emerged as serious candidates for optoelectronic and information technologies. In contrast to TMDCs, layered perovskites not only present unique physics at the monolayer level but also preserve these properties in microscopic thin film devices, such as in solar cells<sup>9,10</sup> and light-emitting diodes<sup>11–15</sup> (LEDs). Notably, hybrid 2D perovskites (2DPVSKs) are able to sustain a large density of current<sup>10</sup> (>100 mA/cm<sup>2</sup>) and yield reasonably high

PLQY values of several to 20%.<sup>12,16,17</sup> However, 2DPVSKs are susceptible to ambient environmental<sup>18</sup> (oxygen, humidity, temperature, etc.) degradation, as compared to purely inorganic materials, which has limited the exploration of their fundamental photophysical properties.

Recent efforts have aimed at exploring their unique physical properties by creating hierarchical stacks of different 2D materials.<sup>19,20</sup> Here, we investigate the physical properties of a new type of vertical heterostructure composed of a few layers of TMDCs and 2DPVSKs. By creating an atomically thin interface between these two types of materials, we were able to identify a two-order of magnitude enhancement in photoluminescence emission and improved air stability as compared to the TMDC and 2DPVSK, respectively. We also investigated the underlying mechanisms for the enhancement in heterostructure photoluminescence with a combination of time-

**Received:** December 22, 2018

**Revised:** June 10, 2019

**Published:** June 24, 2019

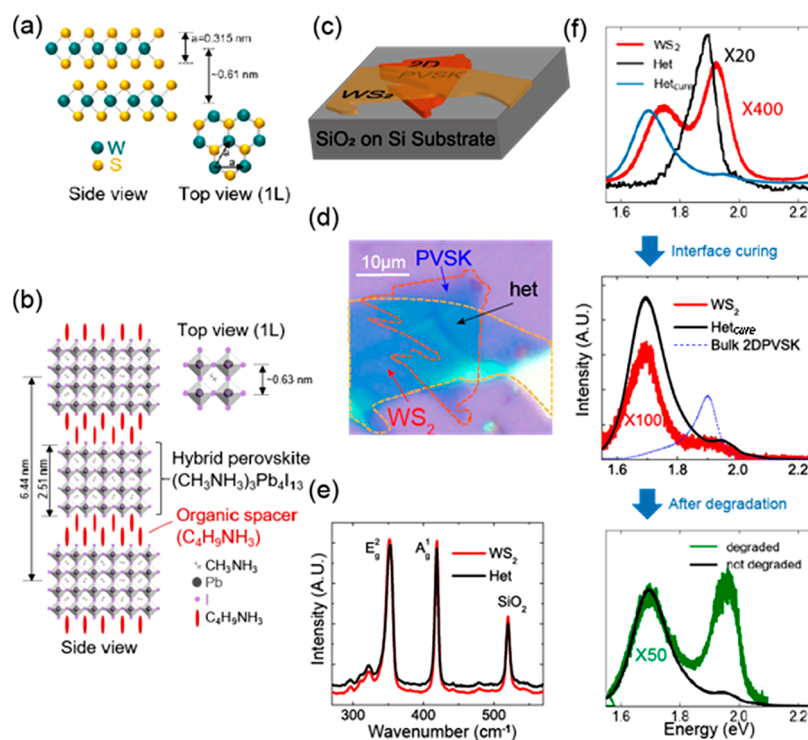


**Figure 1.** Crystal structures and lattice constants of WS<sub>2</sub> (a) and  $n = 4$  2DPVSK (b). (c) Schematic drawing of the heterostructure. (d) Optical image of the 2L WS<sub>2</sub>/ $n = 4$  2DPVSK heterostructure on SiO<sub>2</sub>/Si substrate. (e) Raman spectra of the bare 2L WS<sub>2</sub> and the heterostructure taken in air at room temperature with 514 nm laser excitation. (f) PL spectra of the bare 2L WS<sub>2</sub>, the  $n = 4$  2DPVSK, and heterostructure, measured under ambient atmosphere with 3 kW/cm<sup>2</sup> at 514 nm excitation.

resolved photoluminescence (TRPL) spectroscopy, ultraviolet photoemission spectroscopy (UPS), and materials modeling, where plausible mechanisms for this enhancement is discussed. The giant enhancement of photoluminescence combined with relatively good air stability makes this heterostructure highly promising for ultrathin and ultralight optoelectronic devices. We believe that by creating a functional heterostructure platform combining inorganic and hybrid materials such as TMDCs and 2DPVSKs, this work presents a unique opportunity to quantitatively understand and tailor the interfacial coupling and electronic structure of such dissimilar hierarchical assemblies by tuning the chemical composition, structure, and thickness of each of the materials under external stimuli such as light, electric field, and strain.<sup>15–26</sup>

Figure 1a,b depicts the layered structure of, respectively, the WS<sub>2</sub> TMDC and the Ruddlesden–Popper BA<sub>2</sub>MA<sub>3</sub>Pb<sub>4</sub>I<sub>13</sub> hybrid 2D perovskite (abbreviated as either 2DPVSK or  $n = 4$  in the rest of the text) which are investigated here. The thickness of a single WS<sub>2</sub> and single perovskite layer are 0.315 and 2.51 nm, respectively. For both, strong carrier confinement effects of the layer plane is manifested by a strong anisotropy in optoelectronic and mechanical properties,<sup>10,21</sup> as well as unique photophysics<sup>17,22</sup> such as quantum confinement effects and large exciton binding energies.<sup>23,24</sup> The main difference in the structure of these two materials is that the WS<sub>2</sub> layers are electronically coupled across layers whereas the layers of perovskites are separated from one another by a thin ( $\sim 0.7$  nm) layer of organic materials (butylammonium, BA) and maintain electronic properties of individual layers. The heterostructure (Figure 1c) was constructed by exfoliating 2DPVSK and dry viscoelastic stamping WS<sub>2</sub> on a silicon substrate (Si with a top 285 nm layer of SiO<sub>2</sub>); these processes

took place under inert atmosphere to prevent contamination of the interface and degradation of the 2DPVSK (Supplementary Figure 1). The sample was identified under an optical microscope. Optical image of the sample demonstrates the presence of three regions, bare WS<sub>2</sub>, bare  $n = 4$  2DPVSK, and heterostructure (Figure 1d). From the image optical contrast and Raman spectroscopy (Figure 1e), we conclude that the WS<sub>2</sub> flake is two layers thick and the  $n = 4$  2DPVSK is about three layers thick.<sup>25</sup> The bare WS<sub>2</sub> flake yields Raman resonances at 351 and 418 cm<sup>-1</sup>, corresponding to E<sub>2g</sub> and A<sub>1g</sub> vibration modes, respectively. The 67 cm<sup>-1</sup> separation between the two WS<sub>2</sub> Raman peaks indicates that the WS<sub>2</sub> is double layer (2L).<sup>7</sup> The A<sub>1g</sub> mode is related to out-of-plane vibration of sulfur atoms and is sensitive to doping levels,<sup>26,27</sup> whereas the E<sub>2g</sub> mode is associated with the in-plane vibration of tungsten and sulfur atoms and is sensitive to strain.<sup>28</sup> The heterostructure presents the same Raman spectrum that is almost identical to the bare WS<sub>2</sub> flake within the resolution of our instrument (Figure 1e). These data indicate that the doping level is not significantly altered to be observed in Raman spectra (i.e., a doping of more than  $6 \times 10^{12}$ /cm<sup>2</sup> is needed to register a Raman shift surpassing the instrumental noise), and strain in the WS<sub>2</sub> layers in the heterostructure is unchanged as compared to the WS<sub>2</sub> by itself.<sup>29</sup> On the basis of our fabrication methods, the termination of the 2DPVSK at the interface can take one of several configurations: (i) a single layer of BA molecules (the length of BA is about 0.6 nm) with half the density of that in a BA organic interlayer found in the 2DPVSK; (ii) a layer of iodine atoms with a negative surface charge which we can reasonably exclude on its own from previous theory<sup>30</sup> and the lack of doping observed in the Raman data; or (iii) a missing iodine atom in PbI<sub>2</sub> surface

exposing a Pb<sup>2+</sup> bond.<sup>30</sup> It is also reasonable to expect a nonhomogeneous spatial distribution of the different types of termination enumerated above. The WS<sub>2</sub> is terminated with a layer of S atoms. Depending on the type of termination in the 2DPVSK, the WS<sub>2</sub>/2DPVSK interface thickness could vary<sup>31,32</sup> and display a various degree of hybridization between the WS<sub>2</sub> and 2DPVSK orbitals at their interface.<sup>30,33</sup> Although the lattice constant of the sulfur atom slab is about half the periodic arrangement of the organic BA molecules and perovskite octahedra (Figure 1a,b), the Raman measurements do not indicate any appreciable strain in the WS<sub>2</sub>. This is most likely due to the soft nature of the perovskite and organic layers, as well as the transfer process, which alleviates any significant strain at the interface.<sup>34,35</sup>

Room-temperature photoluminescence (PL) yields significant enhancement of the PL in the heterostructure as compared to the bare WS<sub>2</sub> and 2DPVSK (Figure 1f). Although at first the heterostructure shows a 20-fold enhancement in the PL integrated intensity as compared to the bare 2L WS<sub>2</sub>, we found that after “interface curing” using laser annealing (with a 532 nm laser at a few kW/cm<sup>2</sup> in air for a few minutes) the PL enhancement reaches about 150-fold. After degradation of the sample, the PL intensity decreases by more than 50 times. Before interface curing, the heterostructure yields a single broad emission peak at about 1.9 eV. The bare WS<sub>2</sub> and the heterostructure after interface curing exhibit a broad peak at 1.69 eV and a side feature at higher energy (Figure 1f). The *n* = 4 2DPVSK emits at around 1.9 eV with a low energy shoulder below 1.8 eV. The side feature in WS<sub>2</sub> is also around 1.9 eV, whereas the heterostructure side feature peaks at about 1.95 eV and the main peak in the heterostructure is broader than the bare WS<sub>2</sub>. Again, the main difference between these samples is that the total PL of the heterostructure is enhanced up to 150 times as compared to the bare WS<sub>2</sub>. We also note that the center region of the heterostructure still showed strong emission even after 7 months of storage under nitrogen atmosphere and intermittent exposure to air, whereas luminescence emission from the bare 2DPVSK was not detectable due to sample degradation (Supplementary Figure 2).<sup>18,36</sup> After degradation, we observe a definite decrease in the PL intensity as shown in Figure 1f. More significant decrease of intensity of lower energy peak compared to the 1.9 eV peak indicates that this degradation compromises interfacial interaction achieved through interface curing and is not reversible through further curing process. Our results indicate that WS<sub>2</sub> effectively encapsulates and stabilizes the 2DPVSK underneath it as discussed in the case of boron nitride.<sup>18</sup>

To show that this observation is not limited to the heterostructure in Figure 1, we also investigated the 1L WS<sub>2</sub>/*n* = 3 2DPVSK heterostructure (Supplementary Figure 3). The 1L WS<sub>2</sub>/*n* = 3 heterostructure yielded PL enhancements of about 25 times and 80 times before and after interface curing, respectively. It is important to note that after interface curing, the heterostructure PL spectrum is dominated by a broad feature at about 1.7 eV (Supplementary Figure 3c), which is almost identical to the one observed for the 2L WS<sub>2</sub>/*n* = 4 heterostructure in Figure 1f. Therefore, we infer that the PL feature at ~1.7 eV in the heterostructure of type WS<sub>2</sub>/2DPVSK originates from states located at the heterostructure interface that are strongly activated via interface curing. These PL measurements demonstrate that by combining WS<sub>2</sub> and 2DPVSK in an artificial heterostructure we have obtained

materials with enhanced and more stable PL emission at room temperature.

In order to investigate the mechanism of PL enhancement and understand the features observed at room temperature, we carried out measurements at low temperature (7 K). Differential reflection spectra (defined as  $(I_{\text{sample}} - I_{\text{substrate}})/I_{\text{substrate}}$  shown in Figure 2a) exhibit absorption resonances

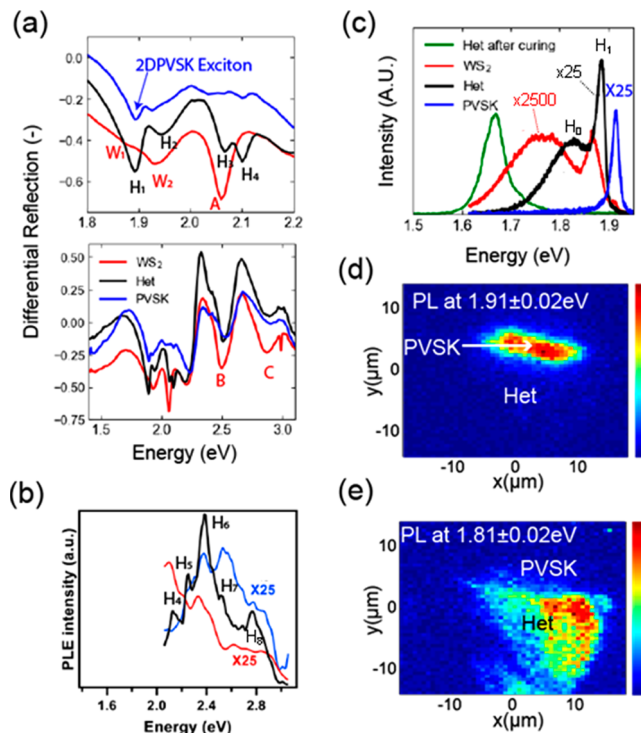


**Figure 2.** Optical properties at 7 K of the 2L WS<sub>2</sub>/*n* = 4 2DPVSK heterostructure compared to the bare WS<sub>2</sub> and *n* = 4 2DPVSK. (a) Reflection spectra. (b) PL excitation spectra. (c) PL spectra taken at 7 K at 550 nm laser excitation with intensity 5W/cm<sup>2</sup> for the bare *n* = 4 and heterostructure, and 900 W/cm<sup>2</sup> for the 2L WS<sub>2</sub>, and 100 W/cm<sup>2</sup> for heterostructure after curing. Intensities are scaled with power and integration time to show relative magnitude. (d) Map of *n* = 4 2DPVSK exciton emission at 900W/cm<sup>2</sup> 550 nm laser excitation with 5 s integration per point. (e) Map of indirect emission of WS<sub>2</sub> at the same condition (color bar in intensity a.u.).

corresponding to the A, B, and C excitons for the bare WS<sub>2</sub>, and the main exciton for the *n* = 4 2DPVSK.<sup>8,23</sup> Additional peaks between 1.85 and 1.95 eV emerging in the bare WS<sub>2</sub> were assigned to the defect states.<sup>37</sup> The bare *n* = 4 2DPVSK exhibits absorption features around 1.95 eV, corresponding to exciton states and higher energy transitions as reported previously.<sup>23</sup> As illustrated in Figure 2a, the reflection spectrum of the heterostructure is not the result of a simple sum of the component WS<sub>2</sub> and 2DPVSK layers, which is confirmed by the optical constants derived from the differential reflection data (Supplementary Figure 4). Precisely, the lowest absorption resonance H<sub>1</sub> in the heterostructure is at the same energy (1.895 eV) as the perovskite exciton peak but with larger amplitude. On the other hand, resonances H<sub>2</sub> (1.945 eV) and H<sub>3</sub> (2.067 eV) are at about the same energy as the absorption peaks W<sub>2</sub> (also corresponding to *n* = 4 exciton excited states) and A in WS<sub>2</sub> but with reduced amplitude. Similarly, higher energy transitions at 2.5 and 2.7 eV corresponding to *n* = 4 feature yield enhanced or similar

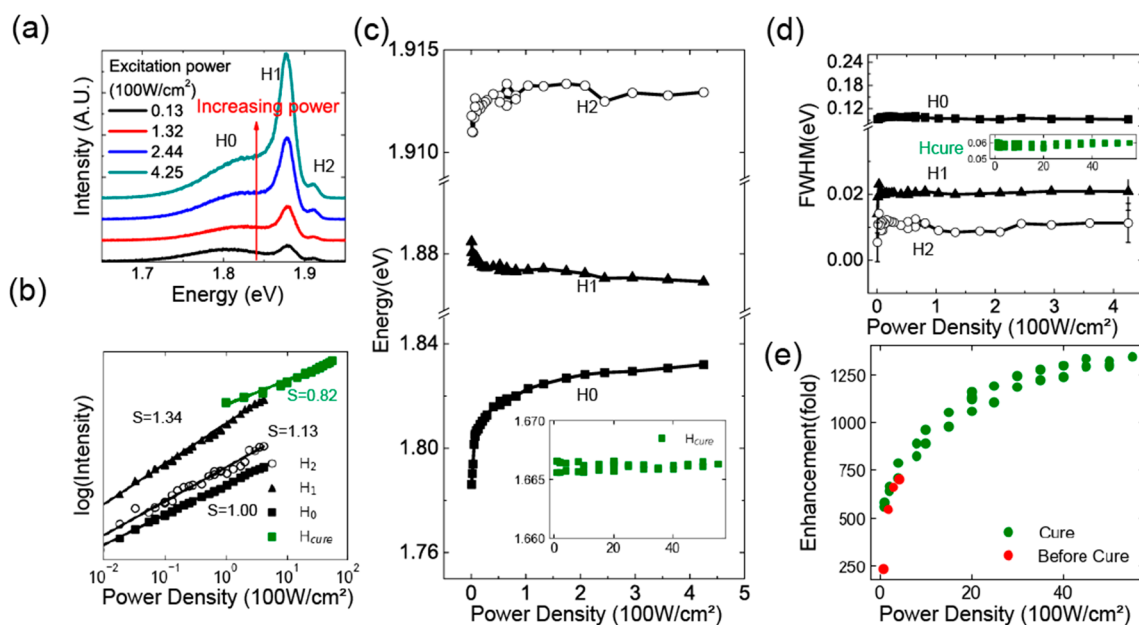


**Figure 3.** Power dependence of PL emission at 7 K. (a) PL spectra of heterostructure taken at different incident laser power. Power dependence of (b) integrated PL intensity and (c) peak position of the PL transitions of the heterostructure. Green squares and line represent the data and fitted line after laser curing. (d) Corresponding power dependent on the fwhm. Inset: data of heterostructure after curing. (e) Enhancement of integrated PL intensity over all energy range measured on heterostructure versus bare WS<sub>2</sub>. The red and green points correspond to before and after curing of the sample.

absorption amplitude as compared to the bare  $n = 4$  2DPVSK. The B and C excitons in the 2L WS<sub>2</sub> are damped in the heterostructure (Supplementary Figure 4). Additionally, we observe a strong resonance peak H<sub>4</sub> at 2.1 eV, which is not clearly present in either of the bare materials, except for a small feature in the bare 2DPVSK spectrum. This new feature was clearly measured using PL excitation (PLE) (Figure 2b). All H<sub>4</sub>, H<sub>5</sub>, and H<sub>6</sub> appear as strong absorption peaks from the PLE data. The most notable observation from the PLE data is the 25-fold enhancement in the heterostructure as compared to the bare WS<sub>2</sub> and  $n = 4$  2DPVSK. Overall, these results can be summarized as the following: the heterostructure absorbs about 25 times more than  $n = 4$  2DPVSK and 2L WS<sub>2</sub>. This is also accompanied (Supplementary Figure 4) by an overall decrease (respectively increase) of the refractive index as compared to the bare WS<sub>2</sub> (respectively  $n = 4$  2DPVSK).

In order to quantify the PL enhancement at low temperature and understand its origin, we analyzed the PL spectra at 7 K. The  $n = 4$  2DPVSK exhibits a single PL peak at 1.91 eV with a Stokes shift of about 40 meV (Figure 2c), which is identified as the exciton ground state.<sup>23</sup> The bilayer WS<sub>2</sub> PL spectrum yields two broad optical transitions: a broad emission at 1.75 eV with full width at half-maximum (fwhm) 105 meV, and a narrower emission line at 1.86 eV (fwhm = 19 meV). We also observed a small side feature at about 1.905 eV depending on the location on the sample (Supplementary Figure 2). On the basis of previous reports,<sup>8,38,39</sup> we attribute the broad emission around 1.75 eV due to defect state emission in bilayer WS<sub>2</sub>. On the other hand, the heterostructure presents a relatively sharp PL peak at 1.87 eV (fwhm = 16 meV) with a broad shoulder around 1.83 eV, which are identified as H<sub>1</sub> and H<sub>0</sub>, respectively. The main change in the heterostructure PL as compared to the individual constituent materials is a 2 orders of magnitude enhancement of the overall PL intensity as compared to the bare WS<sub>2</sub> with a similar emission spectrum (Figure 2c). After interface curing the heterostructure PL

spectrum is dominated by a broad PL peak at 1.65 eV reminiscent of the 1.7 eV PL feature at room temperature. In this case, the heterostructure is enhanced by about 3 orders of magnitude as compared to the bare WS<sub>2</sub> and by 25-fold with respect to the bare  $n = 4$  2DPVSK before curing.

We performed the same study at low temperature on the 1L WS<sub>2</sub>/ $n = 3$  2DPVSK. At 7 K, the monolayer WS<sub>2</sub> yields two emission features, one broad peak at 1.84 eV and a narrow peak at 1.98 eV (Supplementary Figure 3d). These two peaks can be attributed to defect emission, because this emission disappears at room temperature in the bare WS<sub>2</sub>.<sup>8</sup> Here, we observe a 130-fold enhancement in the total PL of the heterostructure as compared to the bare 1L WS<sub>2</sub>, a value on par with the heterostructure 2L WS<sub>2</sub>/ $n = 4$  2DPVSK. The corresponding 50-fold enhancement in the heterostructure PL with respect to the bare  $n = 3$  2DPVSK is larger than in the 2L WS<sub>2</sub>/ $n = 4$  2DPVSK heterostructure but could be explained by the beam damage on 2DPVSK due to prior measurements and different effective light intensity at the substrate surface due to interferences in the SiO<sub>2</sub>. Reflection spectra (Supplementary Figure 3e) show the presence of A and B exciton resonances of the monolayer WS<sub>2</sub> in both the WS<sub>2</sub> and the heterostructure. The ground exciton state of the  $n = 3$  2DPVSK is observed at about 2.0 eV at about the same energy as the W<sub>1</sub> feature of the 1L WS<sub>2</sub>. Overall the reflection spectra leads to the conclusion that the absorption of the heterostructure is dominated by the 1L WS<sub>2</sub> in the low energy range (<2.2 eV), and mainly shows 1L WS<sub>2</sub> features whereas the features of both the  $n = 3$  2DPVSK and 1L WS<sub>2</sub> (B exciton) are observed for energies larger than 2.2 eV. This is confirmed in the PLE spectra (Supplementary Figure 3f). Similar to the 2L WS<sub>2</sub>/ $n = 4$  2DPVSK sample, the PLE spectrum of the 1L WS<sub>2</sub>/ $n = 3$  2DPVSK shows 250 times and 70 times higher PL in heterostructure compared to the bare  $n = 3$  PVS and 1L WS<sub>2</sub> samples, respectively.

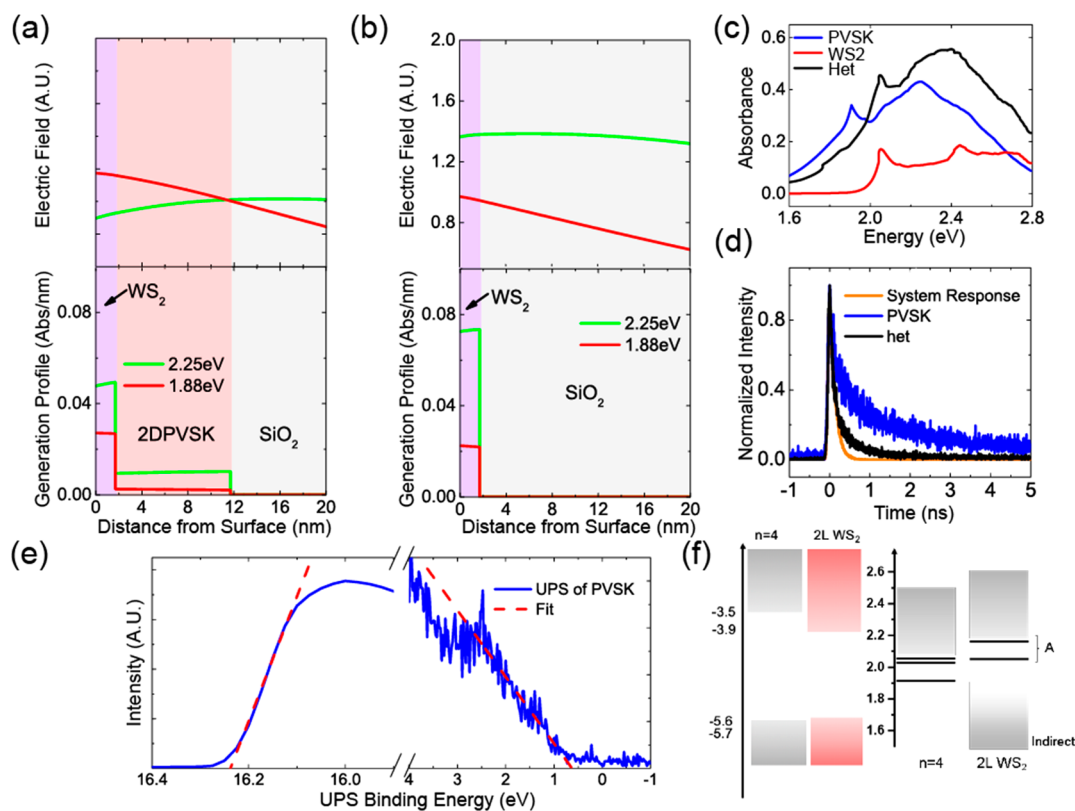


**Figure 4.** Transfer matrix calculation of heterostructure on 285 nm SiO<sub>2</sub> on Si substrate. (a) Generation profile and electric field over depth of heterostructure at excitation emission wavelength in a full heterostructure and (b) WS<sub>2</sub> only sample. (c) Calculated absorption spectra of three regions. (d) Time-dependent photoluminescence spectra of heterostructure and  $n = 4$  2DPVSK taken at 2.25 eV 4.25  $\mu$ W excitation and  $1.88 \pm 0.2$  eV collection. (e) UPS spectra and fitting of  $n = 4$  2DPVSK. (f) Derived band positions of  $n = 4$  2DPVSK and 2L WS<sub>2</sub>, with gray boxes indicating conduction and valence band forming direct band gap, and red box representing indirect band positions. (inset) Energy diagram in the excitonic picture for the bare  $n = 4$  2DPVSK and WS<sub>2</sub> samples taken from previous reports.<sup>23,42,43</sup> Black lines indicate the exciton Rydberg series.

Photoluminescence maps at peak emission energy for the  $n = 4$  2DPVSK and WS<sub>2</sub>, are shown in Figure 2d,e, respectively. At the  $n = 4$  2DPVSK exciton peak (1.91 eV), strong emission of 2DPVSK is only observed in the bare 2DPVSK region, but not in the heterostructure. In contrast, strong defect state emission is observed in the heterostructure region only (1.81 eV). These maps indicate that 2DPVSK emission is quenched under WS<sub>2</sub>. Notice that the emission intensities also exhibit spatial variation over the sample, which can be attributed to spatially inhomogeneous layer thickness and coupling between layers (Supplementary Figure 2).

More insights into the photophysics of the heterostructure were gained by investigating the power dependence of the PL spectra (Figure 3, and Supplementary Figure 5 for the 1L WS<sub>2</sub>/ $n = 3$  heterostructure). The integrated PL of the two peaks H<sub>0</sub> and H<sub>2</sub> yields a close to linear dependence on the light excitation intensity, whereas the main PL feature H<sub>1</sub> presents a superlinear intensity dependence with a coefficient of 1.35 (Figure 3b). Additionally, we observe a  $\sim 40$  meV blueshift of the energy of the PL peak H<sub>0</sub> with increasing excitation intensity (Figure 3c) possibly due to state filling. On the other hand, the PL featuring H<sub>1</sub> undergoes a less than 5 meV redshift over the entire power range and for H<sub>2</sub> we observe a blueshift of less than 2 meV. We also observe no significant broadening of any of the PL features with excitation intensity (Figure 3d). From these results, we conclude that the feature H<sub>0</sub> corresponds to defect bound exciton,<sup>29</sup> which undergoes energy band filling with excitation intensity. Similar

to the WS<sub>2</sub> reflection spectra analysis, the main PL emission H<sub>1</sub> is identified as a biexciton state or mixed excitonic–free carrier states. It is confirmed by the superlinear power dependence of PL intensity.<sup>29</sup> We suggest this may be a signature of a partial dissociation of the exciton at the interface as reported previously for 2DPVSK edge surface or doping at the interface arising from the band alignment and bending. In that case, the redshift with increasing power could be the result of screening effects of the charge interactions at the interface where H<sub>1</sub> state can accumulate, concomitant with the saturation of the H<sub>0</sub> state. In contrast, heterostructure emission after interface curing exhibit slight sublinear power dependence of intensity (coefficient = 0.82), which could be a result of saturation of local states at interface with increasing power. Moreover, its peak position remains unshifted with changing power density, different from defect bound exciton state or indirect transition. This indicates that the PL emission from interface-cured heterostructure has different origin than free excitons or band-to-band transition in 2L WS<sub>2</sub>.

We observe a more than 2 orders of magnitude increase in PL emission in the heterostructure as compared to the bare WS<sub>2</sub> over the applied range of excitation power density. Figure 3e shows that this enhancement factor, corresponding the ratio between the integrated PL in the heterostructure and that in the bare WS<sub>2</sub>, improves from about 220 at 0.8 kW/cm<sup>2</sup> to 700 at 4.4 kW/cm<sup>2</sup>. This improvement is largely attributed to the enhancement of the H<sub>1</sub> state, shown in Figure 3a.

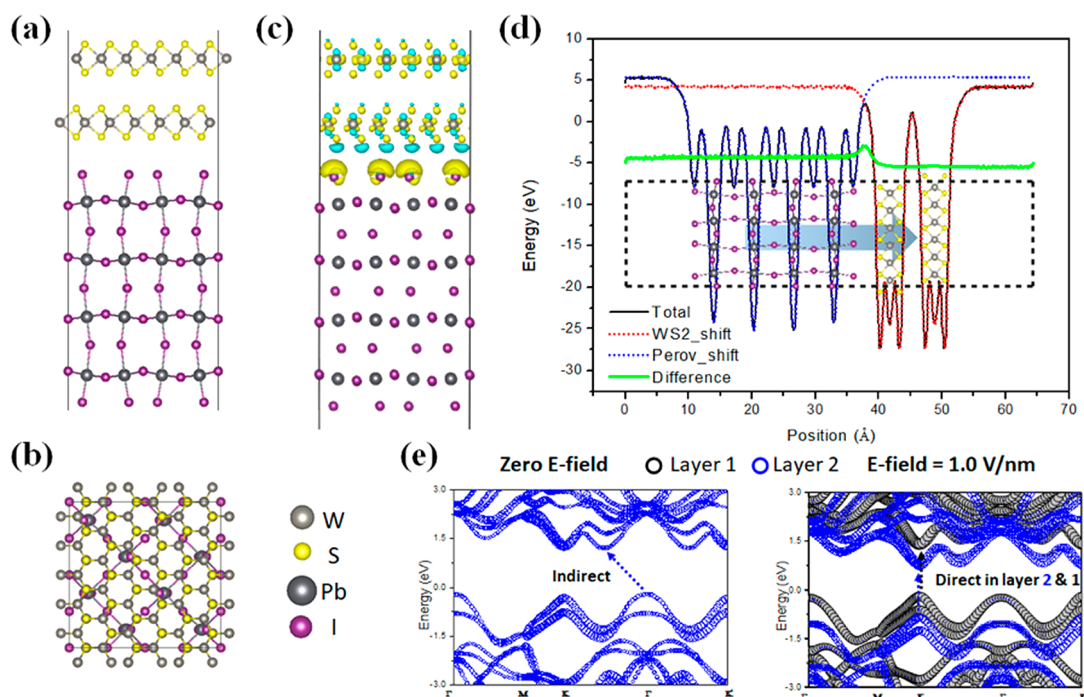


**Figure 5.** DFT calculations of heterostructure of 2L WS<sub>2</sub>/*n* = 4 2DPVSK. (a,b) Side and top view of the heterostructure, respectively. (c) Charge difference distribution of the heterostructure due to the formation of the interface. The yellow and blue colors indicate the electrons and holes, respectively. (d) The plane-averaged potential profile of the heterostructure (black), WS<sub>2</sub> (red), 2DPVSK (blue), and the difference due to the formation of heterostructure (green), respectively. (e) The layer-resolved projected band structures (black and blue circles for two layers) of 2L freestanding WS<sub>2</sub> without (left panel) and with (right panel) E-field demonstrate the indirect-to-direct transition.

To gain a deeper understanding of the PL enhancement in the heterostructures composed of TMDCs and 2DPVSK, we performed TRPL, UPS, and transfer matrix calculations (TMM), Figure 4 and Supplementary Figure 6. TMM calculations indicate that the PL emission enhancement does not originate from an effect of dielectric environment change. Electric field and generation profiles were calculated for the heterostructure and the bare WS<sub>2</sub> at 550 nm (2.25 eV) and 660 nm (1.88 eV), corresponding to the laser excitation wavelength and for the main emission peak (Figure 4a,b). The generation rate per unit length for WS<sub>2</sub> in the heterostructure is higher than from the 2DPVSK in the heterostructure but is nonetheless lower than that of bare WS<sub>2</sub>, indicating the absence of a carrier generation enhancement in WS<sub>2</sub> layer. Calculated absorbance spectra (Figure 4c) indicate that the absorbance of the heterostructure is larger than that of individual layers, but smaller than the sum of absorption from both materials confirming our results in Supplementary Figure 4. Here, A, B, and 2DPVSK exciton peaks observed in reflection measurements (Figure 2a) are consistent with absorption peaks calculated using transfer matrix method while H<sub>4</sub> cannot be explained. TMM calculation also shows 0.45 and 0.15 absorbance of WS<sub>2</sub> A exciton and H<sub>3</sub> peaks, respectively, which is opposite to the reflectance spectra which shows larger dip in WS<sub>2</sub> A exciton, which is likely due to different level of transmission through these two regions and electronic effects. Because transfer matrix calculations do not show either an enhancement of WS<sub>2</sub> emission/absorption or a significant reduction of the *n* = 4 2DPVSK emission/absorption in the heterostructure compared to the individual constituents, purely photonic effects, such as changes in the local dielectric environment, can not fully explain the giant WS<sub>2</sub> PL enhancement. We also confirmed this observation by

exfoliating 2L WS<sub>2</sub> on hexagonal boron nitride (hBN) and BA (Supplementary Figure 7). In both cases, we observe little changes in the PL spectra and no significant photoluminescence enhancement. Figure 4e shows the UPS spectra and spectral fits at the high and low kinetic energy cutoff for the *n* = 4 2DPVSK. The valence band energy for the 2DPVSK obtained from these cut-offs is −5.59 eV referenced to the vacuum level. Literature values for the 2DPVSK band gap and band positions of WS<sub>2</sub>,<sup>23,40–42</sup> indicate that they form a Type I band alignment with an energy level mismatch of about 472 and ~100 meV for the conduction band minimum and valence band maximum, respectively (Figure 4f). We note that the energy difference of the conduction band minima between the 2L WS<sub>2</sub> and *n* = 4 2DPVSK is of the order of the difference between the principle exciton energy in these materials and the 2L WS<sub>2</sub>/*n* = 4 heterostructure PL peak after interface curing. The relatively good energy correspondence between exciton states in both the 2L WS<sub>2</sub> and *n* = 4 2DPVSK might promote dipole–dipole interactions as discussed in ref 43.

TRPL (Figure 4d) measured for the bare 2DPVSK yields a lifetime slightly under the nanosecond time scale in agreement with a previous report.<sup>17</sup> On the other hand, the reported lifetime of bilayer WS<sub>2</sub> is of the order of tens of picoseconds, previously attributed to intervalley scattering.<sup>44</sup> The heterostructure exhibits an intermediate PL decay time between the bare WS<sub>2</sub> and *n* = 4 2DPVSK indicative of either a charge transfer and/or dipole–dipole interactions mechanisms at the interface.<sup>43</sup> This can also be a consequence of the different nature of the photoemitting states at the interface.

The similarities in the results between the two heterostructures support a common mechanism for the origin of the photoluminescence enhancement in TMDCs/2DPVSK heterostructures. We hypothesize that a significant contribution to

the PL enhancement in the heterostructures with respect to their bare constituents is due to their interface. Using first-principles calculation, we verified that the 2L WS<sub>2</sub>/2DPVSK interface modifies the electronic structure of 2L WS<sub>2</sub> and enables large PL enhancement. Microscopic insights about the heterostructures constructed by TMDCs and 2DPVSK have been obtained by first-principles calculation based on density functional theory (see [Supporting Information](#) for calculation details). Heterostructures with different thickness of the 2DPVSK and WS<sub>2</sub> were systematically calculated. [Figure 5a,b](#) shows, respectively, the side and top view of the 2L WS<sub>2</sub>/*n* = 4 2DPVSK structures without the organic ligands. To understand the effect of the heterostructure interface, we first calculated the distribution of the charge transfer between 2L WS<sub>2</sub> and *n* = 4 2DPVSK due to the heterostructure formation. As can be seen in [Figure 5c](#), a clear charge transfer exists between WS<sub>2</sub> and 2DPVSK, where electrons (yellow) and holes (blue) are accumulated at the 2DPVSK and WS<sub>2</sub> side, respectively, and most of the transferred charges (electrons and holes) are distributed near the interface. Therefore, electrons are transferred from 2L WS<sub>2</sub> to 2DPVSK, resulting in the p-doping of the 2L WS<sub>2</sub>. Such p-doping effect could compensate possible n-type doping in the as exfoliated WS<sub>2</sub> samples, leading to the enhancement of formation of exciton and thus the corresponding PL,<sup>8</sup> as observed in the experimental measurements.

On the other hand, due to the charge transfer, an electronic dipole is formed across the heterostructure interface. As can be seen in [Figure 5d](#), the difference of plane-averaged potential at the two sides of the heterostructure (black solid line) confirm the formation of the dipole moment. Moreover, the change of the potential profile due to the heterostructure formation (green solid line in [Figure 5d](#)) shows that potential drop happens mainly across the interface and extends to the 2L WS<sub>2</sub> layers. Such interfacial dipole moment can essentially be considered as an effective electric field (E-field), which is known to alter various properties of 2D layered materials. To better understand such an effect, we can, in a first approximation, study the the electronic properties of a freestanding bilayer WS<sub>2</sub> structure under external E-field. The calculated atom-resolved projected band structure for the two WS<sub>2</sub> layers without and with E-field are summarized in [Figure 5e](#), which shows that the coupled bilayer is electronically decoupled under E-field, behaving as two noninteracting monolayers. Interestingly, a clear indirect-to-direct transition is observed due to such E-field-induced decoupling effect, which contributes to the enormous PL enhancement, consistent with the experimental observations.

From our modelling of TMDC/2DPVSK heterostructures, we found two cooperative effects to contribute to the PL enhancement observed experimentally. These effects are p-doping effect that compensate the n-doping of the as exfoliated WS<sub>2</sub> and E-field induced electronic layer–layer decoupling. It is important to mention that similar charge transfer effect is also observed in heterostructures built by WS<sub>2</sub> and 2DPVSK with different thickness ([Supporting Information](#)). The thicker the 2DPVSK the more charge transfer between the WS<sub>2</sub> and 2DPVSK, vice versa. Considering the E-field induced decoupling effect is only effective to multilayer systems and stronger charge transfer of the 2L WS<sub>2</sub>/*n* = 4 2DPVSK, the PL enhancement of the 2L WS<sub>2</sub>/*n* = 4 2DPVSK is expected to be stronger than that of the 1L WS<sub>2</sub>/*n* = 3 2DPVSK. This is indeed consistent with the 100-fold and 70-fold PL enhance-

ment of the heterostructures 2L WS<sub>2</sub>/*n* = 4 2DPVSK and 1L WS<sub>2</sub>/*n* = 3 2DPVSK, respectively, compared to the WS<sub>2</sub>. We note the interface curing strongly modifies the system, leading to a much larger PL enhancement at a relatively lower energy. The enhancement in PL can be attributed to the reduction in defects, which increases the quantum efficiency of the emission. We anticipate that further theoretical and experimental study will reveal the atomic nature of interfacial structure and the electronic interactions at the interface between TMDCs and 2DPVSKs, which can also participate in the PL enhancement reported in this study.<sup>30,33</sup>

In conclusion, TMDCs and 2DPVSKs have emerged as highly promising materials for optoelectronic applications. However, TMDCs exhibit poor emission due to defect states and direct-to-indirect band transition, and 2DPVSKs suffer from poor stability toward ambient atmosphere. By combining these two materials in vertical heterostructures, we observed a significant enhancement of the photoemission with respect to the bare TMDCs and 2DPVSKs with relatively good stability. The PL enhancement is of the order of 2 orders of magnitude when we compare the heterostructures to the bare TMDCs. First-principles calculations shows that this PL enhancement can be attributed, at least in part, to charge transfer through the interface that generates dipole moment, which induces increased local effective electrical field, and such field results in indirect-to-direct transition of electronic structure of 2L WS<sub>2</sub>. However, electronic coupling at the TMDC/2DPVSK interface cannot be excluded without better understanding of the interface structure. Interestingly the PL emission amplitude and spectral distribution can be altered by interface curing in air under laser excitation, which induces further emission enhancement. The giant enhancement in the PL emission combined with largely improved stability under ambient condition and laser illumination may open opportunities for practical applications of the TMD/2DPVSK heterostructures in high efficiency optoelectronic devices.

## ■ ASSOCIATED CONTENT

### 📄 Supporting Information

The Supporting Information is available free of charge on the [ACS Publications website](#) at DOI: [10.1021/acs.nanolett.8b05105](https://doi.org/10.1021/acs.nanolett.8b05105).

Additional information on experimental details, spatial variation of photoluminescence, measurement on 1L WS<sub>2</sub>/*n* = 3 2DPVSK samples, dielectric functions and photoluminescence excitation spectra, control experiments on WS<sub>2</sub>/hBN and WS<sub>2</sub>/BA samples, and details on first-principle calculations ([PDF](#))

## ■ AUTHOR INFORMATION

### Corresponding Authors

\*E-mail: (A.M.) [adm4@rice.edu](mailto:adm4@rice.edu).

\*E-mail: (H.A.) [haa@caltech.edu](mailto:haa@caltech.edu).

### ORCID

Joelson Wong: 0000-0002-6304-7602

Ellen Yan: 0000-0003-3252-790X

Mercouri G. Kanatzidis: 0000-0003-2037-4168

Deep Jariwala: 0000-0002-3570-8768

Tony Low: 0000-0002-5759-5899

Harry A. Atwater: 0000-0001-9435-0201

**Present Address**

<sup>#</sup>(D.J.) Department of Electrical and Systems Engineering, University of Pennsylvania, Philadelphia, PA 19104, U.S.A.

**Author Contributions**

<sup>†</sup>A.Y. and J.-C.B. contributed equally to this work.

**Notes**

The authors declare no competing financial interest.

**ACKNOWLEDGMENTS**

This work is part of the “Photonics at Thermodynamic Limits” Energy Frontier Research Center funded by the U.S. Department of Energy, Office of Science, Office of Basic Energy Sciences under Award Number DE-SC0019140. We also acknowledge Northrop Grumman for financial support of instrumentation. A.Y. and J.W. acknowledge financial support from a Resnick Institute Fellowship. A.D.M. and J.-C.B. acknowledge support by the DOE-EERE DE-FOA-0001647 program. MGK thanks ONR for support on investigating the stability of 2D perovskites (N00014-17-1-2231). We acknowledge support from the Beckman Institute of the California Institute of Technology to the Molecular Materials Research Center. We are grateful to Prof. George R. Rossman for technical help, discussions, and support. We thank Prof. Jacky Even for useful discussions concerning the perovskite surface termination.

**REFERENCES**

- (1) Palacios-Berraquero, C.; Kara, D. M.; Montblanch, A. R.-P.; Barbone, M.; Latawiec, P.; Yoon, D.; Ott, A. K.; Loncar, M.; Ferrari, A. C.; Atatüre, M. Large-Scale Quantum-Emitter Arrays in Atomically Thin Semiconductors. *Nat. Commun.* **2017**, *8*, 15093.
- (2) Gong, S.-H.; Alpeggiani, F.; Sciacca, B.; Garnett, E. C.; Kuipers, L. Nanoscale Chiral Valley-Photon Interface through Optical Spin-Orbit Coupling. *Science* **2018**, *359* (6374), 443–447.
- (3) Palacios-Berraquero, C.; Barbone, M.; Kara, D. M.; Chen, X.; Goykman, I.; Yoon, D.; Ott, A. K.; Beitner, J.; Watanabe, K.; Taniguchi, T.; et al. Atomically Thin Quantum Light-Emitting Diodes. *Nat. Commun.* **2016**, *7*, 12978.
- (4) Kang, D.-H.; Dugasani, S. R.; Park, H.-Y.; Shim, J.; Gnapareddy, B.; Jeon, J.; Lee, S.; Roh, Y.; Park, S. H.; Park, J.-H. Ultra-Low Doping on Two-Dimensional Transition Metal Dichalcogenides Using DNA Nanostructure Doped by a Combination of Lanthanide and Metal Ions. *Sci. Rep.* **2016**, *6*, 20333.
- (5) Voiry, D.; Yang, J.; Chhowalla, M. Recent Strategies for Improving the Catalytic Activity of 2D TMD Nanosheets Toward the Hydrogen Evolution Reaction. *Adv. Mater.* **2016**, *28* (29), 6197–6206.
- (6) Chen, M.; Xia, J.; Zhou, J.; Zeng, Q.; Li, K.; Fujisawa, K.; Fu, W.; Zhang, T.; Zhang, J.; Wang, Z.; et al. Ordered and Atomically Perfect Fragmentation of Layered Transition Metal Dichalcogenides via Mechanical Instabilities. *ACS Nano* **2017**, *11* (9), 9191–9199.
- (7) Yuan, L.; Huang, L. Exciton Dynamics and Annihilation in WS<sub>2</sub> 2D Semiconductors. *Nanoscale* **2015**, *7*, 7402–7408.
- (8) Zhao, W.; Ghorannevis, Z.; Chu, L.; Toh, M.; Kloc, C.; Tan, P.-H.; Eda, G. Evolution of Electronic Structure in Atomically Thin Sheets of WS<sub>2</sub> and WSe<sub>2</sub>. *ACS Nano* **2013**, *7* (1), 791–797.
- (9) Cao, D. H.; Stoumpos, C. C.; Farha, O. K.; Hupp, J. T.; Kanatzidis, M. G. 2D Homologous Perovskites as Light-Absorbing Materials for Solar Cell Applications. *J. Am. Chem. Soc.* **2015**, *137* (24), 7843–7850.
- (10) Tsai, H.; Nie, W.; Blancon, J.-C.; Stoumpos, C. C.; Asadpour, R.; Harutyunyan, B.; Neukirch, A. J.; Verduzco, R.; Crochet, J. J.; Tretiak, S.; et al. High-Efficiency Two-Dimensional Ruddlesden–Popper Perovskite Solar Cells. *Nature* **2016**, *536* (7616), 312–316.
- (11) Xing, J.; Zhao, Y.; Askerka, M.; Quan, L. N.; Gong, X.; Zhao, W.; Zhao, J.; Tan, H.; Long, G.; Gao, L.; et al. Color-Stable Highly Luminescent Sky-Blue Perovskite Light-Emitting Diodes. *Nat. Commun.* **2018**, *9* (1), 1–8.
- (12) Yuan, M.; Quan, L. N.; Comin, R.; Walters, G.; Sabatini, R.; Voznyy, O.; Hoogland, S.; Zhao, Y.; Beauregard, E. M.; Kanjanaboos, P.; et al. Perovskite Energy Funnel for Efficient Light-Emitting Diodes. *Nat. Nanotechnol.* **2016**, *11* (10), 1–27.
- (13) Lin, K.; Xing, J.; Quan, L. N.; de Arquer, F. P. G.; Gong, X.; Lu, J.; Xie, L.; Zhao, W.; Zhang, D.; Yan, C.; et al. Perovskite Light-Emitting Diodes with External Quantum Efficiency Exceeding 20 per Cent. *Nature* **2018**, *562* (7726), 245–248.
- (14) Yan, F.; Xing, J.; Xing, G.; Quan, L.; Tan, S. T.; Zhao, J.; Su, R.; Zhang, L.; Chen, S.; Zhao, Y.; et al. Highly Efficient Visible Colloidal Lead-Halide Perovskite Nanocrystal Light-Emitting Diodes. *Nano Lett.* **2018**, *18* (5), 3157–3164.
- (15) Tsai, H.; Nie, W.; Blancon, J.-C.; Stoumpos, C. C.; Soe, C. M. M.; Yoo, J.; Crochet, J.; Tretiak, S.; Even, J.; Sadhanala, A.; et al. Stable Light-Emitting Diodes Using Phase-Pure Ruddlesden–Popper Layered Perovskites. *Adv. Mater.* **2018**, *30* (6), 1704217.
- (16) Gong, X.; Voznyy, O.; Jain, A.; Liu, W.; Sabatini, R.; Piontkowski, Z.; Walters, G.; Bappi, G.; Nokhrin, S.; Bushuyev, O.; et al. Electron–Phonon Interaction in Efficient Perovskite Blue Emitters. *Nat. Mater.* **2018**, *17* (6), 550.
- (17) Blancon, J.-C.; Tsai, H.; Nie, W.; Stoumpos, C. C.; Pedesseau, L.; Katan, C.; Kepenekian, M.; Soe, C. M. M.; Appavoo, K.; Sfeir, M. Y. Extremely Efficient Internal Exciton Dissociation through Edge States in Layered 2D Perovskites. *Science* **2017**, *355*, 1288.
- (18) Fang, H. H.; Yang, J.; Tao, S.; Adjokatsé, S.; Kamminga, M. E.; Ye, J.; Blake, G. R.; Even, J.; Loi, M. A. Unravelling Light-Induced Degradation of Layered Perovskite Crystals and Design of Efficient Encapsulation for Improved Photostability. *Adv. Funct. Mater.* **2018**, *28* (21), 1800305.
- (19) Wang, H.; Liu, F.; Fu, W.; Fang, Z.; Zhou, W.; Liu, Z. Two-Dimensional Heterostructures: Fabrication, Characterization, and Application. *Nanoscale* **2014**, *6* (21), 12250–12272.
- (20) Pomerantseva, E.; Gogotsi, Y. Two-Dimensional Heterostructures for Energy Storage. *Nat. Energy* **2017**, *2* (7), 17089.
- (21) Ishihara, T.; Takahashi, J.; Goto, T. Optical Properties Due to Electronic Transitions in Two-Dimensional Semiconductors (CH<sub>2</sub>n + 1NH<sub>3</sub>)PbI<sub>4</sub>. *Phys. Rev. B* **1990**, *42* (17), 11099.
- (22) Mak, K. F.; He, K.; Shan, J.; Heinz, T. F. Control of Valley Polarization in Monolayer MoS<sub>2</sub> by Optical Helicity. *Nat. Nanotechnol.* **2012**, *7* (8), 494–498.
- (23) Blancon, J. C.; Stier, A. V.; Tsai, H.; Nie, W.; Stoumpos, C. C.; Traoré, B.; Pedesseau, L.; Kepenekian, M.; Katsutani, F.; Noe, G. T.; et al. Scaling Law for Excitons in 2D Perovskite Quantum Wells. *Nat. Commun.* **2018**, *9* (1), 1–10.
- (24) Wang, G.; Chernikov, A.; Glazov, M. M.; Heinz, T. F.; Marie, X.; Amand, T.; Urbaszek, B. Colloquium: Excitons in Atomically Thin Transition Metal Dichalcogenides. *Rev. Mod. Phys.* **2018**, *90* (2), 21001.
- (25) Even, J.; Pedesseau, L.; Katan, C. Understanding Quantum Confinement of Charge Carriers in Layered 2D Hybrid Perovskites. *ChemPhysChem* **2014**, *15* (17), 3733–3741.
- (26) Peimyoo, N.; Yang, W.; Shang, J.; Shen, X.; Wang, Y.; Yu, T. Chemically Driven Tunable Light Emission of Charged and Neutral Excitons in Monolayer WS<sub>2</sub>. *ACS Nano* **2014**, *8* (11), 11320–11329.
- (27) Chakraborty, B.; Bera, A.; Muthu, D. V. S.; Bhowmick, S.; Waghmare, U. V.; Sood, A. K. Symmetry-Dependent Phonon Renormalization in Monolayer MoS<sub>2</sub> Transistor. *Phys. Rev. B - Condens. Matter Mater. Phys.* **2012**, *85* (16), 2–5.
- (28) Wurstbauer, U.; Miller, B.; Parzinger, E.; Lin, Z.; Carvalho, B. R.; Kahn, E.; Brien, M. O.; Mcevoy, N.; Motta, C.; Wang, F.; et al. Strain-Induced Phonon Shifts in Tungsten Disulfide Nanoplatelets and Nanotubes. *2D Mater.* **2016**, *4*, 015007.
- (29) He, Z.; Xu, W.; Zhou, Y.; Wang, X.; Sheng, Y.; Rong, Y.; Guo, S.; Zhang, J.; Smith, J. M.; Warner, J. H. Biexciton Formation in Bilayer Tungsten Disulfide. *ACS Nano* **2016**, *10* (2), 2176–2183.

- (30) Volonakis, G.; Giustino, F. Interfaces Between Graphene-Related Materials and MAPbI<sub>3</sub>: Insights from First-Principles. *Adv. Mater. Interfaces* **2018**, *5* (22), 1800496.
- (31) Mao, L.; Ke, W.; Pedesseau, L.; Wu, Y.; Katan, C.; Even, J.; Wasielewski, M. R.; Stoumpos, C. C.; Kanatzidis, M. G. Hybrid Dion-Jacobson 2D Lead Iodide Perovskites. *J. Am. Chem. Soc.* **2018**, *140* (10), 3775–3783.
- (32) Soe, C. M. M.; Stoumpos, C. C.; Kepenekian, M. M.; Traore, B.; Tsai, H.; Nie, W.; Wang, B.; Katan, C.; Seshadri, R.; et al. New Type of 2D Perovskites with Alternating Cations in the Interlayer Space, (C(NH<sub>2</sub>)<sub>3</sub>(CH<sub>3</sub>NH<sub>3</sub>)<sub>n</sub>Pb<sub>n</sub>I<sub>3</sub>N<sup>+</sup>): Structure, Properties, and Photovoltaic Performance. *J. Am. Chem. Soc.* **2017**, *139* (45), 16297–16309.
- (33) Nie, W.; Tsai, H.; Blancon, J.-C.; Liu, F.; Stoumpos, C. C.; Traore, B.; Kepenekian, M.; Durand, O.; Katan, C.; Tretiak, S.; et al. Critical Role of Interface and Crystallinity on the Performance and Photostability of Perovskite Solar Cell on Nickel Oxide. *Adv. Mater.* **2018**, *30* (5), 1703879.
- (34) Ferreira, A. C.; Létoublon, A.; Paofai, S.; Raymond, S.; Ecolivet, C.; Rufflé, B.; Cordier, S.; Katan, C.; Saidaminov, M. I.; Zhumekenov, A. A.; et al. Elastic Softness of Hybrid Lead Halide Perovskites. *Phys. Rev. Lett.* **2018**, *121* (8), 1–6.
- (35) Kepenekian, M.; Traore, B.; Blancon, J. C.; Pedesseau, L.; Tsai, H.; Nie, W.; Stoumpos, C. C.; Kanatzidis, M. G.; Even, J.; Mohite, A. D.; et al. Concept of Lattice Mismatch and Emergence of Surface States in Two-Dimensional Hybrid Perovskite Quantum Wells. *Nano Lett.* **2018**, *18* (9), 5603–5609.
- (36) Fan, Z.; Xiao, H.; Wang, Y.; Zhao, Z.; Lin, Z.; Cheng, H. C.; Lee, S. J.; Wang, G.; Feng, Z.; Goddard, W. A.; et al. Layer-by-Layer Degradation of Methylammonium Lead Tri-Iodide Perovskite Microplates. *Joule* **2017**, *1* (3), 548–562.
- (37) He, Z.; Wang, X.; Xu, W.; Zhou, Y.; Sheng, Y.; Rong, Y.; Smith, J. M.; Warner, J. H. Revealing Defect-State Photoluminescence in Monolayer WS<sub>2</sub> by Cryogenic Laser Processing. *ACS Nano* **2016**, *10* (6), 5847–5855.
- (38) Zhao, W.; Ribeiro, R. M.; Toh, M.; Carvalho, A.; Kloc, C.; Neto, A. H. C.; Eda, G. Origin of Indirect Optical Transitions in Few-Layer MoS<sub>2</sub>, WS<sub>2</sub>, and WSe<sub>2</sub>. *Nano Lett.* **2013**, *13*, 5627–5634.
- (39) Molas, M. R.; Nogajewski, K.; Slobodeniuk, A. O.; Binder, J.; Bartos, M.; Potemski, M. Optical Response of Monolayer, Few-Layer and Bulk Tungsten Disulfide. *Nanoscale* **2017**, *9*, 13128–13141.
- (40) Keyshar, K.; Berg, M.; Zhang, X.; Vajtai, R.; Gupta, G.; Chan, C. K.; Beechem, T. E.; Ajayan, P. M.; Mohite, A. D.; Ohta, T. Experimental Determination of the Ionization Energies of MoSe<sub>2</sub>, WS<sub>2</sub>, and MoS<sub>2</sub> on SiO<sub>2</sub> Using Photoemission Electron Microscopy. *ACS Nano* **2017**, *11*, 8223.
- (41) Guo, P.; Huang, W.; Stoumpos, C. C.; Mao, L.; Gong, J.; Zeng, L.; Diroll, B. T.; Xia, Y.; Ma, X.; Gosztola, D. J.; et al. Hyperbolic Dispersion Arising from Anisotropic Excitons in Two-Dimensional Perovskites. *Phys. Rev. Lett.* **2018**, *121* (12), 127401.
- (42) Li, Y.; Chernikov, A.; Zhang, X.; Rigosi, A.; Hill, H. M.; Van Der Zande, A. M.; Chenet, D. A.; Shih, E. M.; Hone, J.; Heinz, T. F. Measurement of the Optical Dielectric Function of Monolayer Transition-Metal Dichalcogenides: MoS<sub>2</sub>, MoSe<sub>2</sub>, WS<sub>2</sub>, and WSe<sub>2</sub>. *Phys. Rev. B - Condens. Matter Mater. Phys.* **2014**, *90* (20), 1–6.
- (43) Kozawa, D.; Carvalho, A.; Verzhbitskiy, I.; Giustiniano, F.; Miyauchi, Y.; Mouri, S.; Castro Neto, A. H.; Matsuda, K.; Eda, G. Evidence for Fast Interlayer Energy Transfer in MoSe<sub>2</sub>/WS<sub>2</sub> Heterostructures. *Nano Lett.* **2016**, *16* (7), 4087–4093.
- (44) Su, H.; Deng, A.; Zhen, Z.; Dai, J. F.  $\Gamma$ -Valley Assisted Intervalley Scattering in Monolayer and Bilayer WS<sub>2</sub> Revealed by Time-Resolved Kerr Rotation Spectroscopy. *Phys. Rev. B* **2018**, *97* (11), 1–8.